

The fratricide of $\alpha - \Omega$ dynamos by their α^2 siblings

A. Hubbard¹, M. Rheinhardt¹ and A. Brandenburg^{1,2}

¹ Nordita, AlbaNova University Center, Roslagstullsbacken 23, SE-10691 Stockholm, Sweden

² Department of Astronomy, Stockholm University, SE-10691 Stockholm, Sweden

January 12, 2013, Revision: 1.97

ABSTRACT

Context. Helically forced magneto-hydrodynamic shearing-sheet turbulence can support different large-scale dynamo modes, although the $\alpha - \Omega$ mode is generally expected to dominate because it is the fastest growing. In an $\alpha - \Omega$ dynamo, most of the field amplification is produced by the shear. As differential rotation is an ubiquitous source of shear in astrophysics, such dynamos are believed to be the source of most astrophysical large-scale magnetic fields.

Aims. We study the stability of oscillatory migratory $\alpha - \Omega$ type dynamos in turbulence simulations.

Methods. We use shearing-sheet simulations of hydromagnetic turbulence that is helically forced at a wavenumber that is about three times larger than the lowest wavenumber in the domain so that both $\alpha - \Omega$ and α^2 dynamo action is possible.

Results. After initial dominance and saturation, the $\alpha - \Omega$ mode is found to be destroyed by an orthogonal α^2 mode sustained by the helical turbulence alone. We show that there are at least two processes through which this transition can occur.

Conclusions. The fratricide of $\alpha - \Omega$ dynamos by its α^2 sibling is discussed in the context of grand minima of solar and stellar activity. However, the genesis of $\alpha - \Omega$ dynamos from an α^2 dynamo has not yet been found.

Key words. Sun: dynamo – magnetohydrodynamics (MHD)

1. Introduction

The observed existence of large-scale astrophysical magnetic fields, for example galactic or solar fields, is usually explained by self-excited dynamo action within electrically conducting fluids or plasmas. However, this mechanism of field amplification continues to be a matter of debate as the existing theory encounters problems when extrapolated to the large magnetic Reynolds numbers of astrophysics. Nonetheless, large-scale astrophysical fields are believed to be predominately generated by so-called $\alpha - \Omega$ dynamos, in which most of the field amplification occurs through the shearing of field lines by ubiquitous differential rotation, a process known as the Ω effect (Steenbeck & Krause, 1969). For example, many models of the solar dynamo invoke the strong shear found in the tachocline at the base of the convection zone (see, e.g., Charbonneau, 2010). Shear alone cannot drive dynamo action however, and the α effect, caused by helical motions, provides the necessary twist of the sheared field to complete the magnetic field amplification cycle. In the Sun, an α effect is provided via kinetic helicity due to the interaction of stratified convection and solar rotation.

The α effect can drive a dynamo by itself, being then of the so-called α^2 type. These dynamos are of great theoretical interest due to their simplicity, but are expected to be outperformed by $\alpha - \Omega$ dynamos in the wild. Strictly speaking, $\alpha - \Omega$ dynamos should be referred to as $\alpha^2 - \Omega$ dynamos as the α^2 process of course continues to occur in reality, even in the presence of the Ω effect. However, in the mean-field approach one sometimes makes the so-called “ $\alpha - \Omega$ ” approximation by neglecting the production of toroidal field by the α effect entirely in favor of the Ω effect. This also applies to the present paper where we consider numerical solutions of the original equations in three dimensions with turbulent helical flows. However, we will nevertheless refer to $\alpha - \Omega$ and $\alpha^2 - \Omega$ regimes when shear is domi-

nant or comparable with amplification by the helical turbulence, respectively.

Very often, a linear stability analysis of a given setup reveals that several different dynamo modes are expected to be excited at the same time. While during the linear stage the relative strengths of these modes are determined by the initial conditions, the mode or mixture of modes of the final saturated state is decided by the quintessentially nonlinear interactions between the modes in their backreaction on the flow. The naive guess that the final state should always be characterized by the mode with the highest growth rate, has turned out not to be valid in general. In Rädler et al. (1990) it was shown for a mean-field dynamo model with anisotropic α that within the appropriate parameter range both axisymmetric equatorially anti-symmetric and non-axisymmetric equatorially symmetric modes can be stable solutions of the non-linear system. For a system with differential rotation it was also shown there that the stable solution can well be a mixture of axisymmetric and non-axisymmetric modes.

In direct numerical simulations of a geodynamo model with stress-free boundary conditions, it has been observed that again two different dynamo solutions, a dipolar and a “hemispherical” one, can both be stable (Christensen et al., 1999; Grote & Busse, 2000). Because of the free fluid surface in that model, this might even be taken as a hint for the possibility of non-unique stable states in stellar setups as well.

Fuchs et al. (1999) have demonstrated an even more extreme case with a dynamo powered by a forced laminar flow. In the course of the magnetic field growth, the Lorentz force arranges the flow into a different pattern, which is hydrodynamically stable, but unable to drive a dynamo. As the dynamo dies out subsequently without a chance to recover, it was named “suicidal”.

Hence, the question for the character of the final, saturated stage of a dynamo cannot reliably be answered on the basis of a linear approach and the study of the nonlinear model might

unveil very unexpected results. Here, we will show in a simple setup that, while α - Ω dynamos do grow faster than α^2 dynamos, non-linear effects are capable of driving transitions from α - Ω modes to α^2 modes. As the two competing dynamo modes are excited for the same parameter set, i.e., the same eigenvalue problem, we refer to them as *fratricidal*, in reminiscence of the aforementioned suicidal dynamos.

The two astrophysical dynamos for which we have long time-series, the solar dynamo and that of the Earth, both exhibit large fluctuations. The solar dynamo in particular is known to go through prolonged quiescent phases such as the Maunder minimum (Eddy, 1976). A conceivable connection with fratricidal dynamos makes understanding how non-linear effects define large-scale dynamo magnetic field strengths and geometries a matter of more than intellectual curiosity.

In Section 2 we sketch the mean-field theory of α^2 and α^2 - Ω dynamos. In Section 3 we describe our numerical set-up and briefly discuss the test-field method, a technique to extract the turbulent transport coefficients of mean-field theory from direct numerical simulations. In Sections 4 and 5 we describe different transition types, and we conclude in Section 6.

2. Mean field modeling

In the magneto-hydrodynamic approximation, the evolution of magnetic fields is controlled by the induction equation

$$\frac{\partial \mathbf{B}}{\partial t} = \nabla \times (\mathbf{U} \times \mathbf{B} - \eta \mathbf{J}), \quad (1)$$

where \mathbf{B} is the magnetic field, $\mathbf{J} = \nabla \times \mathbf{B}$ is the current density in units where the vacuum permeability is unity, and η is the microphysical resistivity. A common approach to (1) is mean-field theory, under which physical quantities (upper case) are decomposed into mean (overbars) and fluctuating (lower case) constituents:

$$\mathbf{B} = \overline{\mathbf{B}} + \mathbf{b}. \quad (2)$$

The mean can be any which obeys the Reynolds averaging rules, and is frequently assumed to be a spatial one filtering out large length-scales (a two-scale approach). Here we will however use planar averaging, either over the xy plane so that $\overline{\mathbf{B}} = \langle \mathbf{B} \rangle_{xy} = \overline{\mathbf{B}}(z) \equiv \overline{\mathbf{B}}^Z$ or over the yz plane, that is, $\overline{\mathbf{B}} = \langle \mathbf{B} \rangle_{yz} = \overline{\mathbf{B}}(x) \equiv \overline{\mathbf{B}}^X$, where $\langle \cdot \rangle_\xi$ denotes averaging over all values of the variable ξ (or volume, if not specified). A mean defined by averaging over y only will also be used.

Under Reynolds averaging Eq.(1) becomes

$$\frac{\partial \overline{\mathbf{B}}}{\partial t} = \nabla \times (\overline{\mathbf{U}} \times \overline{\mathbf{B}} + \overline{\mathbf{E}} - \eta \overline{\mathbf{J}}), \quad (3)$$

$$\frac{\partial \mathbf{b}}{\partial t} = \nabla \times (\overline{\mathbf{U}} \times \mathbf{b} + \mathbf{u} \times \overline{\mathbf{B}} + \mathbf{u} \times \mathbf{b} - \overline{\mathbf{E}} - \eta \mathbf{j}), \quad (4)$$

where $\overline{\mathbf{E}} \equiv \overline{\mathbf{u} \times \mathbf{b}}$ is the mean electromotive force (EMF) associated with correlations of the fluctuating fields.

Symmetry considerations allow one to write the $\overline{\mathbf{E}}$ as a function of the mean-fields in the system. In the case of a planar averaging scheme, the equation becomes

$$\overline{\mathbf{E}}_i = \alpha_{ij} \overline{B}_j - \eta_{ij} \overline{J}_j + \dots, \quad (5)$$

where α_{ij} and η_{ij} are turbulent transport coefficients, and averaged quantities depend on one spatial coordinate only. The traditional α effect is described by the symmetric part of the tensor α_{ij} , and requires helicity in the flow. The symmetric part of

η_{ij} describes turbulent dissipation, and, in the isotropic case, appears equivalently to the microphysical resistivity η . It is therefore termed the *turbulent resistivity*, η_t . When assuming that $\overline{\mathbf{E}}$ can be completely represented by the mean magnetic field and its first spatial derivatives, the Taylor series in (5) can be truncated after the term $\eta_{ij} \overline{J}_j$. A more complete formula would include higher spatial as well as temporal derivatives.

2.1. Mean-field dynamo action

Let us assume a large-scale shearing flow of the simple form

$$\mathbf{U}_S = S x \hat{\mathbf{y}}. \quad (6)$$

and velocity fluctuations which are isotropic, homogeneous, and statistically stationary. Consequently, if α_{ij} and η_{ij} are assumed to be independent of $\overline{\mathbf{B}}$ (the kinematic limit), then they reduce to constant scalars α and η_t ¹.

If this system were to contain a y -dependent mean field, the shear would induce field constituents which are proportional to x . We restrict ourselves here to periodic spatial dependencies and hence exclude such unbounded fields. The evolution of harmonic mean magnetic fields is given by the solution of the eigenvalue problem

$$\lambda \hat{\mathbf{B}} = \begin{pmatrix} -\eta_T k^2 & -i\alpha k_z & 0 \\ i\alpha k_z + S & -\eta_T k^2 & -i\alpha k_x \\ 0 & i\alpha k_x & -\eta_T k^2 \end{pmatrix} \hat{\mathbf{B}}, \quad (7)$$

where $\overline{\mathbf{B}} = \hat{\mathbf{B}} \exp(i\mathbf{k} \cdot \mathbf{x} + \lambda t)$, $\eta_T = \eta_t + \eta$, and $k^2 = k_x^2 + k_z^2$. The resulting dispersion relation reads

$$(\lambda + \eta_T k^2)[(\lambda + \eta_T k^2)^2 - \alpha^2 k^2 + i\alpha S k_z] = 0, \quad (8)$$

with eigenvalues (apart from the always decaying modes with $B_y = 0$)

$$\lambda_{\pm} = -\eta_T k^2 \pm (\alpha^2 k^2 - i\alpha S k_z)^{1/2}. \quad (9)$$

It can easily be seen that there are two “pure” modes with particularly simple geometries: the α^2 mode with $k_z = 0$ does not depend on S and has the form

$$\hat{\mathbf{B}}^{\alpha\alpha} = B^{\alpha\alpha} (0, \sin k_x x, \pm \cos k_x x), \quad (10)$$

where the growth rate is $\lambda^{\alpha\alpha} = |\alpha k_x| - \eta_T k_x^2$ and $B^{\alpha\alpha}$ is an amplitude factor. The upper (lower) sign corresponds to positive (negative) αk_x .

In contrast, the α^2 - Ω mode with $k_x = 0$ does depend on S and has, for $S \gg \alpha k_z$ (the α - Ω approximation) the form

$$\hat{\mathbf{B}}^{\alpha\Omega} = B^{\alpha\Omega} \left(\sin[k_z(z - ct)], \sqrt{2} \left| \frac{c}{\alpha} \right| \sin[k_z(z - ct) + \phi], 0 \right), \quad (11)$$

$$c = \text{sign}(\alpha S) \sqrt{|\alpha S / 2k_z|}. \quad (12)$$

In the above $B^{\alpha\Omega}$ is, again, an amplitude factor, ϕ represents, for $S > 0$ ($S < 0$), the $\pm\pi/4$ ($\pm 3\pi/4$) phase shift between the x and y components of the mean field, and upper (lower) signs apply for positive (negative) values of αk_z ; see Table 3 of Brandenburg & Subramanian (2005). The corresponding growth rate is

$$\Re\{\lambda^{\alpha\Omega}\} = \sqrt{|\alpha S k_z|/2} - \eta_T k_z^2. \quad (13)$$

¹ Strictly speaking, shear could introduce anisotropy felt by mean fields with non-vanishing z -components. Our results do not reveal any such.

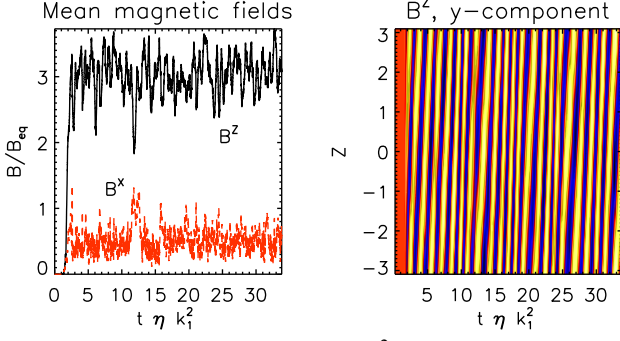


Fig. 1. Time series for a dominantly α^2 - Ω dynamo with $\text{Re}_M = 20$, $\text{Pr}_M = 5$ and $k_f \approx 3.1$. Left: rms value of $\bar{\mathbf{B}}^Z$ defined as $\langle \bar{\mathbf{B}}^{Z^2} \rangle_z^{1/2}$, to be associated with the α^2 - Ω mode (black/solid), and of $\bar{\mathbf{B}}^X$, defined as $\langle \bar{\mathbf{B}}^{X^2} \rangle_x^{1/2}$, to be associated with the α^2 mode (red/dashed). Right: butterfly diagram of $\bar{\mathbf{B}}_y^Z$ showing the dynamo wave of the α^2 - Ω mode.

For equal $|\mathbf{k}|$, the α - Ω mode grows faster than the α^2 mode.²

A key characteristic of α^2 - Ω solutions is that the growth rate λ has a non-vanishing imaginary part $k_z c$ which results in traveling waves with phase speed c . The wave nature of α^2 - Ω solutions is a significant draw in explaining the oscillatory solar magnetic cycle. For a characteristic α^2 - Ω dynamo found numerically with a setup described below, we show in Fig. 1 the time-series of rms values of \mathbf{B} alongside the traveling wave in the z - t plane (“butterfly diagram”). This solution is similar to those considered recently by Käpylä & Brandenburg (2009). There are other sources for such oscillations however. Admittance of a spatially varying α enables oscillatory and hence traveling wave solutions in pure α^2 dynamos, see Baryshnikova & Shukurov (1987), Rädler & Bräuer (1987), Stefani & Gerbeth (2003), Mitra et al. (2010).

The mean fields of α^2 modes are force free, while α^2 - Ω modes cause a potential force which has minimal effect as long as the peak Alfvén speed is sub-sonic. Within kinematics, the induction equation allows for superimposed α^2 and α^2 - Ω modes and in Section 4 we will discuss the interactions within such a superposition.

3. Model and Methods

3.1. Numerical setup

We have run simulations of helically forced sheared turbulence in homogeneous isothermal triply (shear) periodic cubic domains with sides of length 2π . The box wavenumber, which is also the wavenumber of the observed mean fields, is therefore $k_1 = 1$. Unless otherwise specified, our simulations have 64^3 grid points. For the shear flow we have taken the one defined by

² When assuming both k_x and k_z to be different from zero, but keeping the α - Ω approximation valid and k_z fixed, the phase speed of the dynamo wave does not change while the growth rate is reduced by ηk_x^2 . However, the eigenmode has now a z component $\sim -k_x/k_z \bar{\mathbf{B}}_x$. Such modes were not observed in our simulations.

(6). We solve the non-dimensionalized system

$$\frac{\partial \mathbf{A}}{\partial t} = \mathbf{U} \times \mathbf{B} + \eta \nabla^2 \mathbf{A} \quad (14)$$

$$\frac{D\mathbf{U}}{Dt} = -c_s^2 \nabla \ln \rho + \frac{1}{\rho} \mathbf{J} \times \mathbf{B} + \mathbf{F}_{\text{visc}} + \mathbf{f}, \quad (15)$$

$$\frac{D \ln \rho}{Dt} = -\nabla \cdot \mathbf{U}, \quad (16)$$

where $c_s = 1$ is the isothermal sound speed, ρ the density, $\mathbf{F}_{\text{visc}} = \rho^{-1} \nabla \cdot (2\rho \nu \mathbf{S})$ the viscous force, $\mathbf{S}_{ij} = \frac{1}{2}(U_{i,j} + U_{j,i}) - \frac{1}{3}\delta_{ij} \nabla \cdot \mathbf{U}$ is the rate of strain tensor, ν is the kinematic viscosity and \mathbf{f} the forcing term. We use the PENCIL CODE³, which employs sixth-order explicit finite differences in space and a third order accurate time stepping method. While our code allows full compressibility the simulations are only weakly compressible (small Mach number). As in earlier work (Brandenburg, 2001), in each time step the forcing function is a snapshot of a circularly polarized plane wave. All these waves have the same handedness, but their direction and phase change randomly from one time step to the next. This forcing provides kinetic helicity. The wavevectors are taken from the set of vectors that satisfy periodicity and whose moduli are adequately close to the target forcing wavenumber k_f .

The magnetic vector potential is initialized with a weak Gaussian random field, the initial velocity is given by $\mathbf{U} = \mathbf{U}_S$ and the initial density is uniform. In Table 1 we have collected the control parameters and some key derived quantities of the model. Two parameters of note are the magnetic Reynolds and Prandtl numbers,

$$\text{Re}_M = u_{\text{rms}}/\eta k_f, \quad \text{Pr}_M = \nu/\eta. \quad (17)$$

To characterize the turbulence, we provide values of α and η_t which characterize the corresponding tensors as described in Section 2. These were determined using the test-field method with test-field wavevector $\mathbf{k} = \hat{x}$ or $\mathbf{k} = \hat{z}$.

For our purposes, we require the helical turbulence to be strong enough that the α^2 dynamo can safely be excited. For this we guaranteed that in all our simulations, Re_M is above the critical value (of the order of unity) for α^2 dynamos in the corresponding *shearless* setup. Further, some of the transitions we will study require long simulation times due to their rarity, which constrains us to modest numerical resolutions. This in turn prevents our (explicit) numerical resistivity from being small, so the turbulent velocities must be reasonably large for the stated super-critical values of Re_M . Choosing furthermore subsonic shear speeds, we are restricted to a modest region of

³ <http://pencil-code.googlecode.com>

Table 1. Control and derived parameters

ν	Control par.	Microphysical viscosity
η	Control par.	Microphysical resistivity
S	Control par.	Shear ($\mathbf{U}_S = S x \hat{y}$)
f_{rms}	Control par.	Forcing amplitude
k_f	Control par.	Forcing wavenumber (generally $k_f \approx 3.1$)
Pr_M	ν/η	magnetic Prandtl number
u_{rms}	$\langle \mathbf{u}^2 \rangle^{1/2}$	RMS turbulent velocity
Re_M	$u_{\text{rms}}/\eta k_f$	Magnetic Reynolds number
k_1	$k_1 = 1$	Wavenumber of mean fields (box wavenumber)
t_{res}	$1/\eta k_1^2$	Resistive time (mean fields)
t_{turb}	$1/u_{\text{rms}} k_f$	Turbulent time

parameter space. In light of these limitations we operate mostly in a $\text{Pr}_M > 1$ regime.

3.2. Test-field method

A fundamental difficulty in extracting the tensors α_{ij} and η_{ij} from a numerical simulation of (14)–(16) is that (5) is underdetermined. Turbulent transport depends on the velocity field, so “daughter” simulations of the induction equation, whose velocity fields are continuously copied from the main run, share the same tensors α_{ij} and η_{ij} . It is therefore possible to lift the degeneracy by running an adequate number of daughter simulations with suitably chosen “test” mean fields. We employ this *test-field method* (TFM); for an in depth overview see Schrunner et al. (2005, 2007) and Brandenburg et al. (2008a,b). Recently the original method has been extended to systems with rapidly evolving mean-fields, requiring a more complicated *ansatz* than Eq. alphaeta (Hubbard & Brandenburg, 2009) and to the situation with magnetic background turbulence (Rheinhardt & Brandenburg, 2010).

In addition to calculating planar-averaged turbulent tensors as described in the references above, we will be interested in tensors that depend both on x and z (that is, are y -averages). For this, we generalize (5) to

$$\bar{\mathcal{E}}_i = \alpha_{ij} \bar{B}_j + \beta_{ijk} \frac{\partial \bar{B}_j}{\partial x_k} + \dots \quad (18)$$

There are 27 tensor components (as $\partial_y \bar{\mathbf{B}} = \mathbf{0}$), so nine test-fields are required, which we choose to be of the form

$$\mathbf{B}^{pq} = B^T f_q(x, z) \delta_{ip} \hat{\mathbf{e}}_i, \quad p = 1, 2, 3, \quad q \in \{\text{cc}, \text{sc}, \text{cs}\}, \quad (19)$$

where $f_q(x, z)$ is defined, according to the choice of q , to be one of the following functions:

$$\cos k_1 x \cos k_1 z, \quad \sin k_1 x \cos k_1 z, \quad \cos k_1 x \sin k_1 z,$$

and B^T is, as standard for test-field methods, an arbitrary amplitude factor. Although the wavenumber of the test fields is usually treated as a varying parameter we need here to consider only the single value k_1 because the fastest growing and also the saturated dynamos in the simulations are dominated by this wavenumber, the smallest possible in our periodic setup. As is often the case in applications of the test-field method, we will occasionally be faced with unstable solutions of the test problems. We treat that difficulty by periodically resetting the test solutions (see Hubbard et al., 2009). Since it takes a finite time for the test solutions to reach their stationary values, and as this time is frequently close to the required reset time, only limited windows in the time series of the data are valid.

4. Dynamical interactions of α^2 and α^2 - Ω modes

Here we report on the results of our simulations a first set of which is characterized in Table 2. In Figure 2 we show time series for Run A, which saw a transition from a z -varying α^2 - Ω dynamo (\bar{B}^Z) to an x -varying α^2 dynamo (\bar{B}^X). As is made clear in the bottom panel, there was a prolonged period where the two modes were coexisting while their relative strengths were changing monotonically. However, note that B_y^X is stronger than B_z^X , that is, the α^2 field is distorted during the transition. Run A was repeated 16 times with the same parameters, but different random seeds, and all these runs exhibited similar behavior.

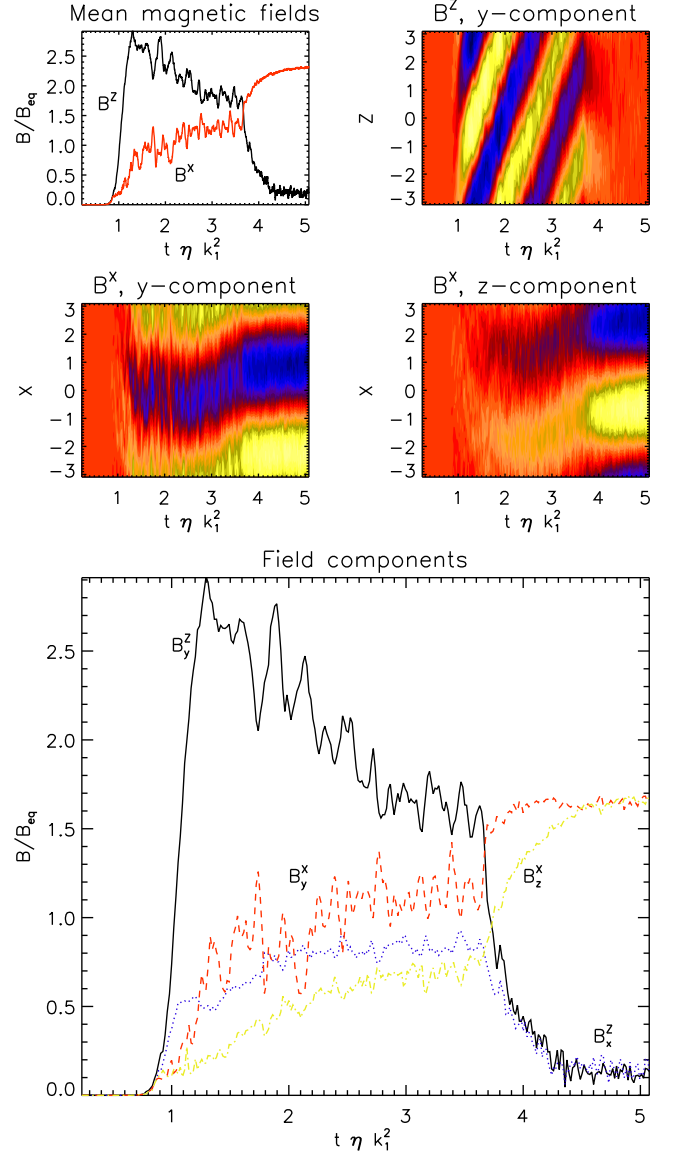


Fig. 2. Time series for Run A. Upper row: same quantities as in Fig. 1. Middle row: \bar{B}_y^X and \bar{B}_z^X , to be associated with the α^2 mode. Note that the α^2 - Ω and α^2 modes coexist during the transition. Lower panel: rms values of the components of $\bar{\mathbf{B}}^X$ and $\bar{\mathbf{B}}^Z$.

Likewise we performed runs where both the value of η and the numerical resolution (cf. Runs B-D, I,J) were varied. As these additional runs also showed the same transition pattern, we conclude that it is deterministic for this level of shear and forcing. More, we conclude that for these cases the α^2 - Ω mode is unstable to the growth of an α^2 mode due to non-linear effects. Runs with the dynamical parameters (S , u_{rms}) of Table 2 inevitably generate α^2 fields from α^2 - Ω fields after modest times, runs with significantly different parameters will usually (for most of the random seeds) exit the kinematic regime into an α^2 - Ω mode, and stay in that mode for a prolonged time with no sign of an α^2 field. Nonetheless even such simulations can occasionally fail to fully enter in the α^2 - Ω regime, instead exiting the kinematic regime into an α^2 mode, as shown in Figure 3.

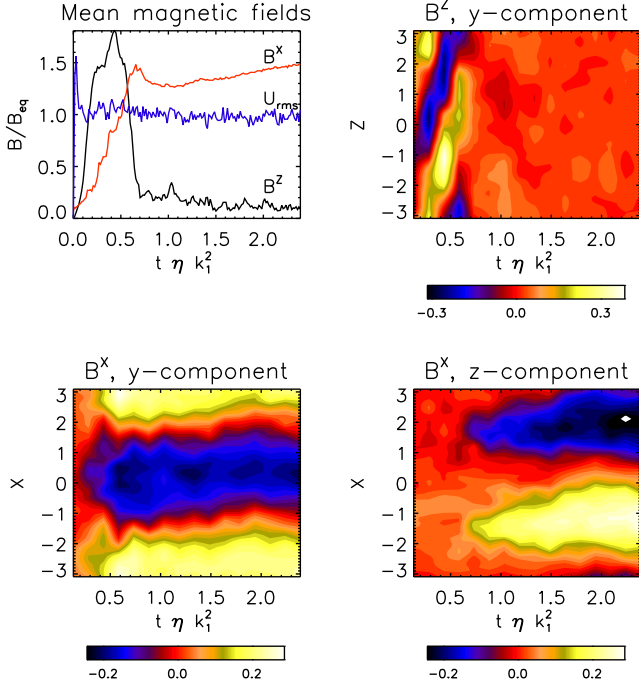


Fig. 3. Time series for Run E that never entered a quasi-stationary α^2 - Ω regime. Top left: rms values of \overline{B}^Z to be associated with the α^2 - Ω mode (black) and of \overline{B}^X to be associated with the α^2 mode (red). Note the considerably faster growth of the α^2 - Ω mode during the kinematic phase. Top right: Butterfly diagram of \overline{B}_y^Z , showing the traveling dynamo wave during the kinematic phase only, but later merely fluctuations. Bottom: components of \overline{B}^X .

4.1. Mean-field approach

Clearly, the transition from an α^2 - Ω mode to an α^2 one must be a consequence of the back-reaction of $\overline{\mathbf{B}}$ onto the flow. Within the mean-field picture, there are two channels available for it: (i) the back-reaction onto the fluctuating flow, usually described as a dependence of α_{ij} (more seldom η_{ij}) on the mean field and (ii) the back-reaction onto the mean flow by the mean Lorentz force, which might again be decomposed into a part resulting from the fluctuating field, $\overline{\mathbf{j}} \times \overline{\mathbf{b}}$, and one resulting from the mean

field, $\overline{\mathbf{j}} \times \overline{\mathbf{B}}$. Here, we will deal with a flow generated by the latter force that straddles the distinction of means and fluctuations: it survives under y -averaging, but vanishes under the xy and yz averaging that reveals the α^2 - Ω and α^2 dynamos respectively. For simplicity we consider magnetic field configurations that would result from a superposition of linear modes of the α - Ω and α^2 dynamos, given in equations (11) and (10) respectively. Such a situation will inevitably occur during the kinematic growth phase if both dynamos are supercritical, but is only relevant for analyzing the back-reaction onto the flow if it at least to some extent continues into the non-linear regime. Our analysis is linear in nature, so while it provides a qualitative framework for understanding the transition process, it is surely not quantitatively accurate.

In order to be able to consider both \overline{B}^X and \overline{B}^Z as mean fields under one and the same averaging, we have now to resort to y averaging. Moreover, for the sake of clarity we will occasionally subject the resulting x and z dependent mean fields further to spectral filtering with respect to these coordinates. That is, we will consider only their first harmonics $\sim e^{ik_1(x+z)}$ as mean fields.

Let us represent the mean field $\langle \mathbf{B} \rangle_y$ as superposition of a \overline{B}^X resembling the (x varying) α^2 mode $\overline{B}^{a\alpha}$ (Eq. (10)) and a \overline{B}^Z resembling the (z varying) α - Ω mode $\overline{B}^{a\Omega}$ (Eq. (11)):

$$\begin{aligned} \overline{B}^Z &= B^Z \begin{pmatrix} \sin(k_1 z') \\ G \sin(k_1 z' + \phi) \\ 0 \end{pmatrix}, \quad \overline{\mathbf{j}}^Z = k_1 B^Z \begin{pmatrix} -G \cos(k_1 z' + \phi) \\ \cos(k_1 z') \\ 0 \end{pmatrix}, \\ \overline{B}^X &= B^X \begin{pmatrix} 0 \\ H \sin k_1 x \\ \cos k_1 x \end{pmatrix}, \quad \overline{\mathbf{j}}^X = k_1 B^X \begin{pmatrix} 0 \\ \sin k_1 x \\ H \cos k_1 x \end{pmatrix}, \end{aligned} \quad (20)$$

with $z' \equiv z - ct$ recalling that c is the speed of the dynamo wave (Eq. (12)). In the above, $\pi/4 \leq \phi \leq 3\pi/4$ and $G, H, k_1 > 0$ are appropriate for $\alpha > 0$. The parameters G and H capture the difference in the strengths of the y and z components (α^2) or the x or y components (α^2 - Ω), respectively. We expect $G > 1$ as shear amplifies the y component of an α^2 - Ω mode well above its x component. The inclusion of the parameter H , which is unity for pure α^2 modes will be justified below, but can already be seen in the different strengths shown in Figure 2, lower panel.

The mean Lorentz force $\overline{\mathbf{j}} \times \overline{\mathbf{B}}$ for the superimposed fields can be written as

$$\begin{aligned} \overline{\mathbf{F}}_L &= \langle \mathbf{F}_L \rangle_y = \\ &= k_1 B^X B^Z \cos k_1 x [G \cos(k_1 z' + \phi) + H \sin(k_1 z')] \hat{y} + \nabla \Phi. \end{aligned} \quad (21)$$

As the Mach numbers were found to be small throughout, we assume incompressibility and hence drop the potential component $\nabla \Phi$. Further, we assume that $\overline{\mathbf{F}}_L$ and the mean velocity driven by it are simply linked by a coefficient $K \approx 1/\nu_T k_1^2$, where the total viscosity ν_T is the sum of the molecular ν , and the turbulent viscosity ν_t . Thus we can approximate the mean velocity due to the interaction of the superimposed mean fields as

$$\overline{\mathbf{U}}_L = U_L \cos k_1 x [G \cos(k_1 z' + \phi) + H \sin(k_1 z')] \hat{y}, \quad (22)$$

where $U_L = K k_1 B^X B^Z$. Clearly, this flow, having merely a y component, shows quadrupolar geometry in the x - z plane as $\overline{U}_{L,y}$ can be rewritten in the form $U'_L \cos k_1 x \cos(k_1 z' + \phi')$ with a new amplitude and phase, U'_L and ϕ' .

The simulations show indeed a dominant part of that shape in the Lorentz-force generated mean flow as can be seen from Figure 4. There the y -averaged U_y is shown together with its Fourier constituent $\sim e^{ik_1(x+z)}$. The latter contains approximately

Table 2. Run parameters

Run	Res.	$-S$	u_{rms}	$-\alpha^\dagger$	η_t^\dagger	Re_M	Pr_M	τ^\ddagger
Run A	64^3	0.05	0.11	0.04	0.025	37	5	2-3
Run B	64^3	0.05	0.17	0.04	0.03	26	2.5	2
Run C	128^3	0.05	0.14	0.04	0.027	44	3	4
Run D	128^3	0.05	0.14	0.04	0.027	90	6	1.5
Run E	64^3	0.02	0.13	0.04	0.023	90	10	N/A
Run I	64^3	0.05	0.15	0.04	0.036	49	1	3
Run J	64^3	0.05	0.19	0.04	0.035	31	0.5	1.5

Notes. \dagger Time-averaged values determined through the TFM using harmonic test fields with $\mathbf{k} = \hat{x}$ or $\mathbf{k} = \hat{z}$. The results are identical due to homogeneity of the time-averaged turbulent velocity. $\ddagger \tau = t_{\text{dur}}/t_{\text{res}}$ is the duration of the transition of the type discussed in Section 4; counting from multiple random seeds for Run A.

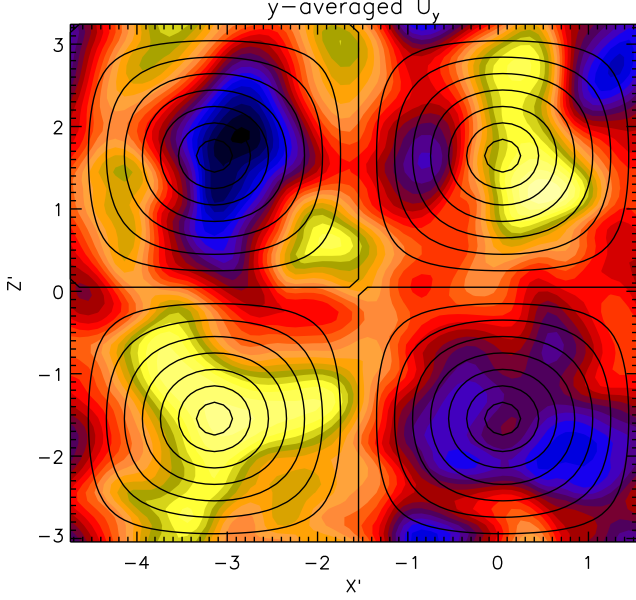


Fig. 4. $\langle U_y \rangle_y$ for Run A, taken at early time ($t = 1.45t_{\text{res}}$) when $\bar{\mathbf{B}}^X$ is still of only modest strength. Plotting area is shifted in x and z to make the quadrupolar geometry clear. Overplotted contours: quadrupolar constituent $\sim \cos k_1 x' \cos k_1 z'$

10% of the energy in this component, or $U'_L = \bar{U}_{y,\text{rms}}/3$, indicating that the assumptions made in deriving (22) are reasonably well justified in a non-linear system.

Upon interaction with a $\bar{\mathbf{B}}^X$ or a $\bar{\mathbf{B}}^Z$ of the form (20), the mean flow $\bar{\mathbf{U}}_L$ in (22) generates an $\bar{\mathcal{E}}_x(z)$ and $\bar{\mathcal{E}}_z(x)$, respectively.

4.2. Dominating α^2 - Ω mode

If $B^Z \gg B^X$, then $\bar{\mathbf{B}}^X$ can be treated as a perturbation, and we can drop higher order terms in B^X . Accordingly, the z -averaged EMF due to the flow $\bar{\mathbf{U}}_L$ is

$$\mathcal{E}^X = \langle \bar{\mathbf{U}}_L \times \bar{\mathbf{B}}^Z \rangle_z = \frac{Kk_1}{2} B^X B^{Z2} (G \sin \phi - H) \cos k_1 x \hat{z}. \quad (23)$$

The curl of this EMF is

$$\nabla \times \mathcal{E}^X = B^X I \sin(k_1 x) \hat{y}, \quad I \equiv \frac{Kk_1^2 B^{Z2}}{2} (G \sin \phi - H). \quad (24)$$

If $G \sin \phi > H$, then $I > 0$ and for $H > 0$ this EMF reinforces $\bar{\mathbf{B}}^X = B^X H \sin k_1 x$. Thus we see that the inclusion of the parameter H in the ansatz for $\bar{\mathbf{B}}^X$, Eq. (20), was justified as $\bar{\mathbf{B}}^X$ receives enhanced forcing in comparison to $\bar{\mathbf{B}}^Z$.

4.3. Dominating α^2 mode

If $B^X \gg B^Z$ then we can in turn treat $\bar{\mathbf{B}}^Z$ as a perturbation. Further, as the system is dominated by the α^2 mode, we will have $H \sim 1$. In this case we find

$$\begin{aligned} \mathcal{E}^Z &= \langle \bar{\mathbf{U}}_L \times \bar{\mathbf{B}}^X \rangle_x \\ &= \frac{Kk_1}{2} B^Z B^{X2} [G \cos(k_1 z' + \phi) + H \sin(k_1 z')] \hat{x}, \end{aligned} \quad (25)$$

and

$$\nabla \times \mathcal{E}^Z = B^Z \frac{Kk_1^2}{2} B^{X2} [H \cos(k_1 z') - G \sin(k_1 z' + \phi)] \hat{y}. \quad (26)$$

We can write

$$\begin{aligned} H \cos(k_1 z') - G \sin(k_1 z' + \phi) = \\ [(H \cos \phi - G) \sin(k_1 z' + \phi)]_1 + [H \cos \phi \cos(k_1 z' + \phi)]_2. \end{aligned} \quad (27)$$

If $H \cos \phi - G < 0$, as expected since $H \sim 1$, $G > 1$, term $[\]_1$ in (27) will act to damp $\bar{\mathbf{B}}^Z$, that is, the perturbative α^2 - Ω wave. Further, term $[\]_2$ is opposite in sign to the time-derivative of such a wave, so it slows or reverses the direction of wave-propagation.

4.4. Mean-Field Evolution

Here we assume again domination of the α^2 - Ω mode, that is, $B^Z \gg B^X$. With Eqs. (7) and (24) the eigenvalue problem for the modified α^2 field $\bar{\mathbf{B}}^X$ is then (adopting $k_x = k_1$, $k_z = 0$)

$$\lambda^X \bar{\mathbf{B}}^X = \begin{pmatrix} -\eta_T k_1^2 & 0 & 0 \\ S & -\eta_T k_1^2 & -i(\alpha k_1 + I) \\ 0 & i\alpha k_1 & -\eta_T k_1^2 \end{pmatrix} \bar{\mathbf{B}}^X, \quad (28)$$

with eigenvalues

$$\lambda^X = -\eta_T k_1^2 \pm \sqrt{\alpha k_1 (\alpha k_1 + I)}. \quad (29)$$

Making the approximation $I \gg \alpha k_1$, similar to the α - Ω approximation $S \gg \alpha k_1$, we find

$$\lambda^X = -\eta_T k_1^2 \pm \sqrt{\alpha I k_1}. \quad (30)$$

The above should be compared with the growth rate of the α - Ω dynamo, $\lambda^{\alpha\Omega}$ from (13) which is not touched by the occurrence of I . The α - Ω dynamo saturates when α has been quenched such that the product αS settles at the marginal value $|\alpha S| = 2\eta_T^2 |k_1|^3$. If the parameter I becomes comparable with the shear, i.e., $I \sim S$, then $\bar{\mathbf{B}}^X$ might grow even when the α^2 - Ω field is saturated, i.e. $\lambda^X > \Re(\lambda^{\alpha\Omega}) = 0$. In other terms, the α^2 - Ω mode is unstable to the growth of a *fratricidal* α^2 field, so the transition will take a well defined time from the onset of the non-linear stage, determined by λ^X .

We test this theory for Run A at the time of Fig. 4, $t = 1.45t_{\text{res}}$, extracting G and H from the relative strengths of the x and y or y and z components of the averaged fields $\bar{\mathbf{B}}^Z$ or $\bar{\mathbf{B}}^X$, respectively, after a projection onto the first harmonics; see Eq. (20). The parameter I is calculated from the magnetic and velocity fields using

$$I = \frac{k_1 B^Z U_L}{2B^X} (G \sin \phi - H), \quad (31)$$

with $U_L = U'_L / \sqrt{G^2 + H^2 - 2GH \sin \phi}$, where U'_L is the amplitude of the quadrupolar constituent of the velocity field seen in Fig. 4. We find $U'_L \simeq 0.07$, $H \simeq 2.9$, $G \simeq 4.9$, $I \simeq 0.09$, and confirm that $\phi \simeq \pi/4$. As $I > S = 0.05$, the growth of the x -varying mode even when the α - Ω mode is saturated is not surprising. Repeating this run (keeping the control parameters fixed) 16 times with different random seeds changed the occurrence time of the transition by only one resistive time, suggesting that the transition is an essentially deterministic process.

We have never seen a reverse transition from the α^2 state back to the α^2 - Ω state. This may be understood in terms of interacting modes, with the α^2 - Ω mode being suppressed once the α^2 mode is dominating; see Sec. 4.3.

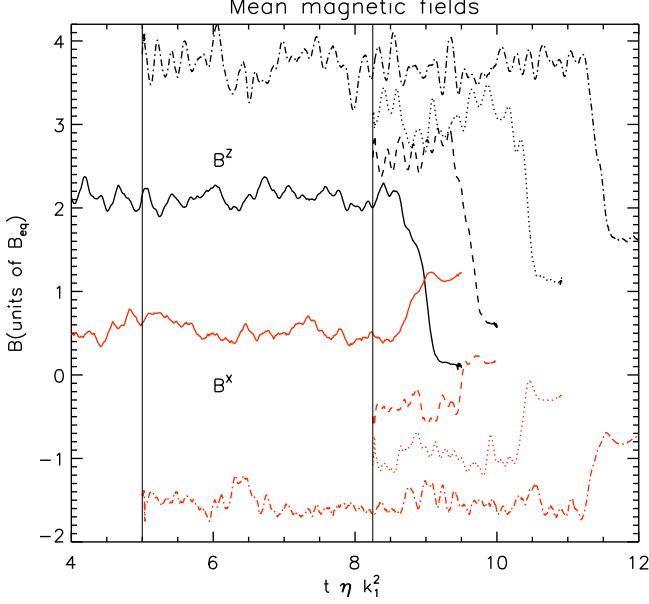


Fig. 5. Time series for Run F (solid lines), with rms values of \overline{B}^Z (black) and \overline{B}^X (red). Broken lines: restarts from the main run with new random seeds, vertically offset for visibility. All the runs end up with the same energies in \overline{B}^X and \overline{B}^Z . Vertical lines: restart times.

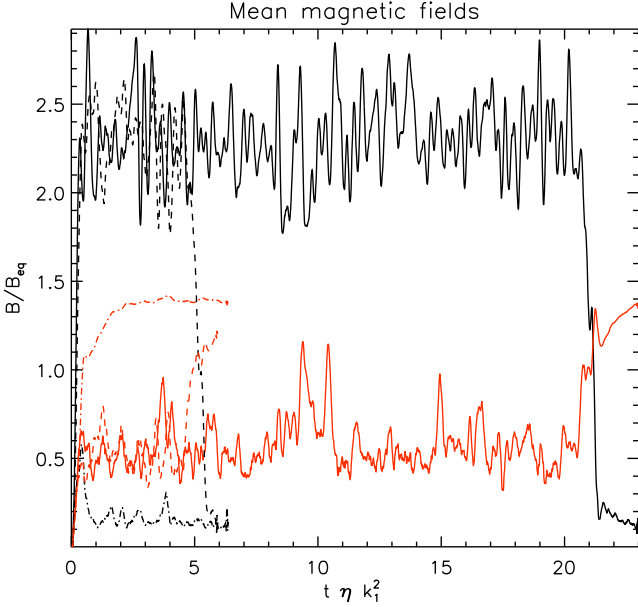


Fig. 6. Time series of Run G (solid) along with a sibling run (dashed) with different seeds, showing significant differences in the transition start time. Dash-dotted: a run which never entered the α^2 – Ω regime.

Table 3. Run parameters

Run	Res.	$-S$	u_{rms}	$-\alpha^\dagger$	η_t^\dagger	Re_M	Pr_M	τ^\ddagger
Run F	64^3	0.2	0.14	0.02	0.1	90	10	$5, 9^\ddagger$
Run G	64^3	0.2	0.099	0.01	0.16	63	10	$5, 20^\ddagger$
Run H	64^3	0.1	0.085	0.017	0.037	27	5	25

Notes. † see Table 2. $^\ddagger \tau = t_{\text{trans}}/t_{\text{res}}$ is the time when transition occurred; for F and G over multiple realizations with differing random seeds. See Fig. 7.

5. Random transitions

Not all transitions fit the above deterministic picture of interacting α^2 – Ω and α^2 modes. In Fig. 5 we present a set of time series of the rms values of \overline{B}^Z and \overline{B}^X , all related to Run F of Table 3. Secondary runs were performed by branching off from the original simulation either at $t = 5t_{\text{res}}$, when the α^2 – Ω mode is well established and stationary, or at $t = 8.25t_{\text{res}}$, immediately before the transition to the α^2 mode is launched. The only difference between all these runs is in the random seed, which is used by the forcing algorithm. In all, the time until the transition starts varies by $\approx 2.5t_{\text{res}}$, and many more turbulent turnover times ($\text{Re}_M k_f^2/k_1^2 \approx 800$ turbulent turnover times per resistive time). The time elapsed during a transition is always of the order of $t_{\text{res}}/2$, unlike $3t_{\text{res}}$ for the process seen in Fig. 2. Thus it is suggestive to assume that there might be a very slow, still essentially deterministic process, preparing the transition, which is likely resistive in nature as that is the longest obvious “native” timescale of the system. Slow resistive effects are known to exist in dynamos, for example the slow resistive growth of α^2 dynamos in periodic systems. However, transitions can indeed occur at very different times including the extreme case in which a run never develops a quasi-stationary α^2 – Ω mode, but instead enters the α^2 state almost immediately after the end of the kinematic phase, see Fig. 6 (run G of Table 3). We believe therefore that under certain circumstances the transition process is not a deterministic one, in that it is impossible to predict or at least estimate the time until the transition. Figure 7 is a synopsis of simulations that belong to that type, hence do not show the instability discussed in Section 4. Note that, while corresponding setups without shear are known to enable α^2 modes for the entire parameter range, the α^2 mode is possibly sub-critical for $\text{Re}_M = 10$, $S = -0.1$.

This is different from the interacting mode picture of Sec. 4 in several interesting ways. Firstly, the α^2 – Ω mode is here at least meta-stable against growth of the α^2 mode, as evinced by its prolonged life-time (hundreds of turbulent times) and the small magnitude of \overline{B}^X , which further is not dominated by a α^2 mode. A reasonable working hypothesis for the cases of Sec. 4 is then that, there, the α^2 mode is the only stable solution and, as soon as the nonlinear stage has been entered, it starts to devour the α^2 – Ω one, settling after a time which is related to basic parameters of the system and hence not random. In contrast, for the cases considered here, we conclude that both the α^2 and the α^2 – Ω solutions are indeed stable (not only metastable) and the latter has a well extended basin of entrainment. Due to its higher growth rate the system settles first in the α^2 – Ω mode and suppresses the α^2 mode efficiently. A transition to the latter can only occur if a random fluctuation in the forcing is strong enough to push the system over the separatrix into the basin of entrainment of the α^2 mode. This can happen after a rather long time only or immediately after the end of the linear stage which has both been observed.

Given that the examples for the first scenario (Table 2) differ from those for the second (Table 3) mainly in their lower rate of shear, our conclusion seems reasonable as stronger shear should result in a clearer preference of the α^2 – Ω mode as the α^2 mode does not feel the shear. Or, in other terms, from a certain shear rate S on, the α^2 – Ω mode should acquire a basin of entrainment with a finite “volume” that grows with S . If this picture is true, transitions in the two scenarios should have clearly different characteristics, and indeed, the transition in Fig. 5 is markedly faster than that seen in Fig. 2.

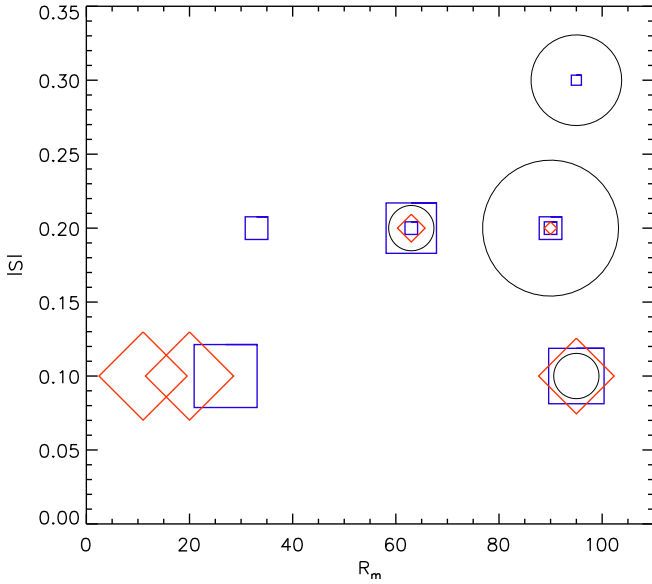


Fig. 7. Synopsis of runs which did not exhibit the instability discussed in Section 4. Runs at the same position differ only in random seeds. Circles/black: a significant α^2 - Ω mode was never developed (cf. Fig. 3), size indicates the corresponding number of runs (1, 2 or 3). Square/blue: a transition occurred, size represents the time until transition (4 to $25t_{\text{res}}$). Diamond/red: the α^2 - Ω stage was entered, but no transition occurred. Size represents the time span of simulation (5 to $35t_{\text{res}}$).

As in the transitions discussed in Sec. 4, we have not here seen the α^2 mode transit back into the α^2 - Ω mode. Some attempts were made to provoke this reverse transition by perturbing the α^2 state with a (sufficiently strong) α^2 - Ω mode. While in some runs it indeed took over, velocities were attained for which the numerics are unreliable, and often proved numerically unstable, making the results inconclusive. However, such a behavior is not entirely surprising as the α^2 - Ω saturation process can anyway be somewhat wild, cf. Fig. 3.

The absence of *spontaneous* reverse transitions appears plausible insofar the time variability of the α^2 mode is much smaller than that of the α^2 - Ω mode, which can clearly be seen in Fig. 8 for Run H. That is, events capable of pushing the system over the separatrix are simply much rarer. Significantly longer integration times are likely needed for their eventual detection, but it is also conceivable that the triggering event never shows up.

5.1. Large scale patterns

Run H will be examined here in more detail. Curiously, $\langle U_y \rangle_y$ taken just during the transition as shown in Fig. 9 does not show the quadrupolar pattern of Fig. 4. It is therefore not surprising that the butterfly diagrams in Fig. 10 do not show a direct transition from the α^2 - Ω to the α^2 dynamo, as \overline{B}_z^X develops significantly later than \overline{B}_y^X . This is clearly visible in Fig. 8, lower panel. As consideration of the mean flow due to the Lorentz force of the mean field alone is obviously not fruitful in explaining this transition, we recall that the back-reaction of the mean field onto the turbulence opens another channel of nonlinear interaction.

According to elementary mean-field dynamo theory, the α effect is caused by the helicity in the flow: $\alpha \sim \langle \mathbf{w} \cdot \mathbf{u} \rangle$, where $\mathbf{w} \equiv \nabla \times \mathbf{u}$ is the fluctuating vorticity. Further, the back-reaction of the mean field on the turbulence, which saturates the dynamo,

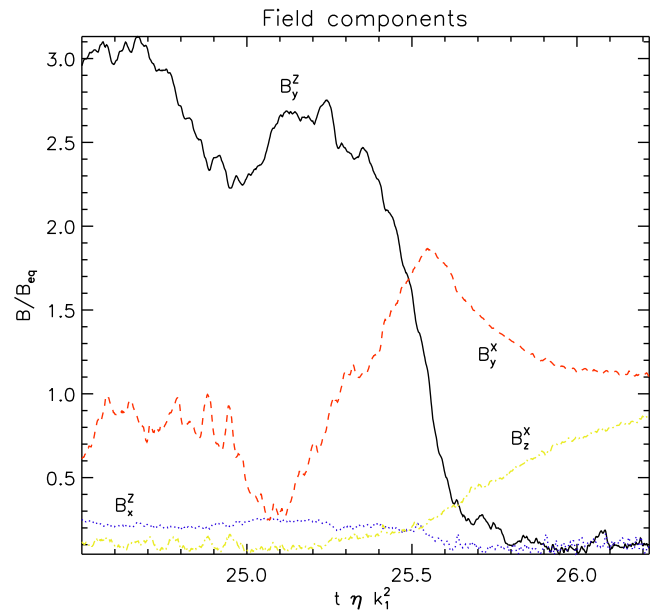
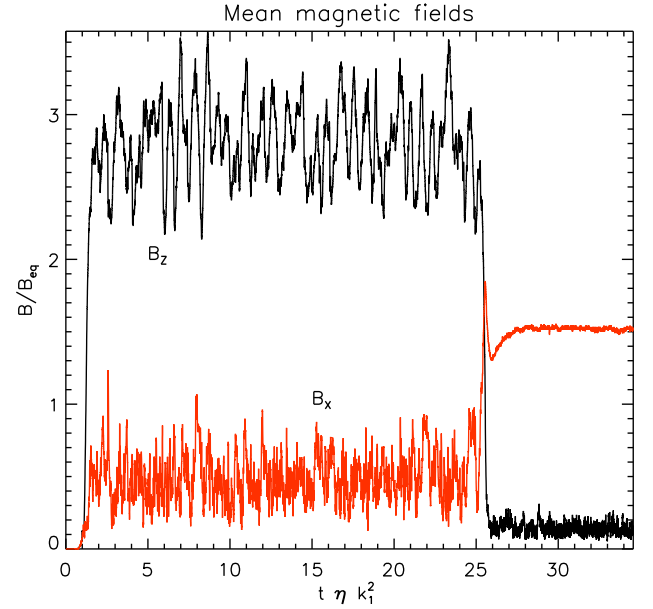


Fig. 8. Time series of Run H. Upper panel: rms values of \overline{B}^X and \overline{B}^Z . Note the long time before the transition starts in comparison to Run F (see Fig. 5) and the dramatic difference in the fluctuation levels before and after the transition. Lower panel: rms values of the components. Note the strong difference between \overline{B}_y^Z and \overline{B}_x^Z , expected for an α^2 - Ω field. More significantly, notice that \overline{B}_y^X develops before \overline{B}_z^X .

is assumed to be captured by the current helicity $\langle \mathbf{j} \cdot \mathbf{b} \rangle$. It is often related to the magnetic helicity $\langle \mathbf{a} \cdot \mathbf{b} \rangle$ and thought to reduce the original α by producing a *magnetic* contribution of opposite sign. In Fig. 11 we present time-series of the power spectra of these helicity correlators across the transition. We see no clear signal around the transition event.

5.2. Mean-field modeling with y averaging

To examine the problem more closely, we recall Eq. 18 for when the mean is defined by a y average:

$$\mathcal{E}_i(x, z) = \alpha_{ij}(x, z)\overline{B}_j(x, z) + \beta_{ijk}(x, z)\overline{B}_{j,k}(x, z). \quad (32)$$

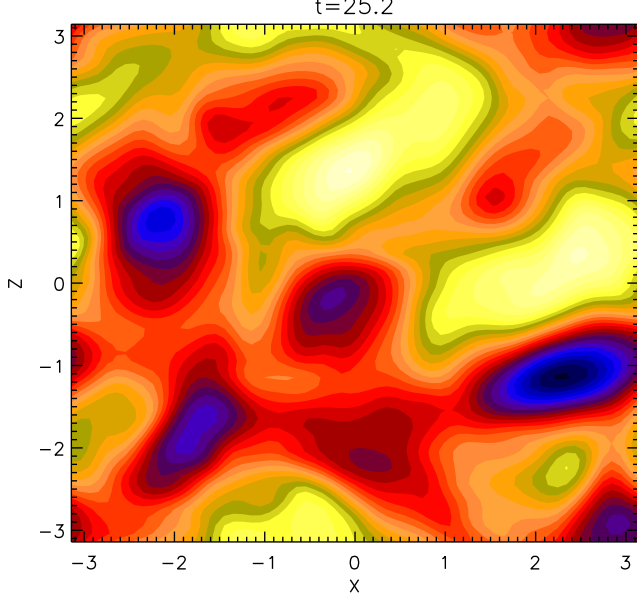


Fig. 9. $\langle U_y \rangle_y$ taken during the transition of Run H shown in Fig. 8 ($t = 25.2t_{\text{res}}$). Note the lack of a quadrupolar geometry.

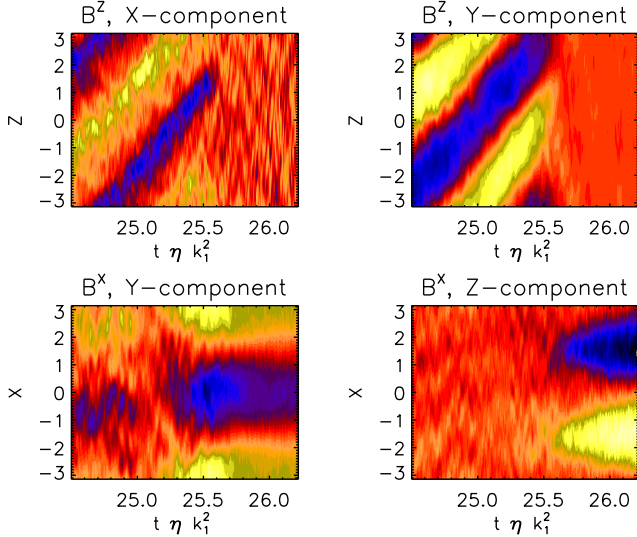


Fig. 10. Butterfly diagrams for Run H, (see Fig. 8). Note that \overline{B}_y^X develops before \overline{B}_z^X , i.e., \overline{B} does not transit from an α^2 - Ω field straight to an α^2 one.

It is clear that the Fourier constituents of α_{ij} and β_{ijk} with wavenumber k_1 in both x and z (the quadrupolar constituents) can create an emf \mathcal{E}^X out of a field \overline{B}^Z , both with the same wavenumber:

$$\overline{\mathcal{E}}_i^X = \left\langle \alpha_{i1}^{11} \overline{B}_x^Z + \alpha_{i2}^{11} \overline{B}_y^Z + \beta_{i13}^{11} \frac{\partial \overline{B}_x^Z}{\partial z} + \beta_{i23}^{11} \frac{\partial \overline{B}_y^Z}{\partial z} \right\rangle_z, \quad (33)$$

where the superscripts indicate the coefficients to be the Fourier constituents $\sim e^{ik_1(x+y)}$ and \overline{B}_z^Z is assumed to vanish. Note that each of them is actually given by four values, e.g., the two amplitudes and phases in:

$$\alpha_{ij}^{11} = \alpha_{ij}^c \cos(k_1 x + \phi_{ij}^c) \cos k_1 z + \alpha_{ij}^s \cos(k_1 x + \phi_{ij}^s) \sin k_1 z. \quad (34)$$

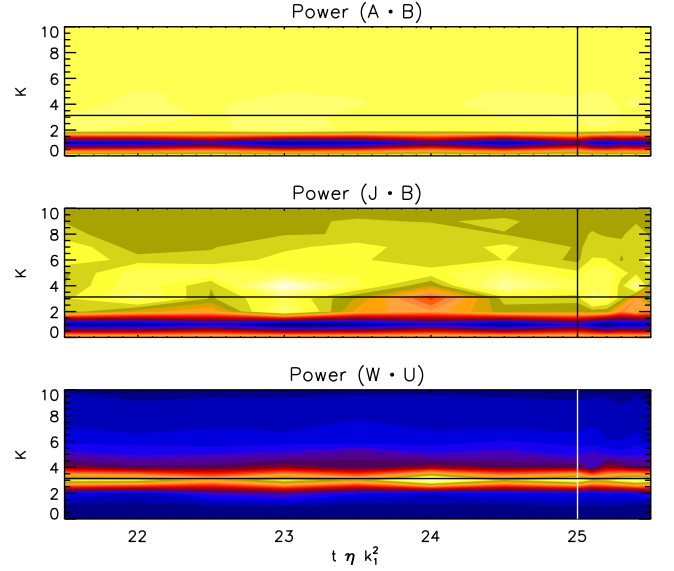


Fig. 11. Time series of the helicity power spectra for Run H. Horizontal line: forcing wavenumber $k_f \approx 3.1$. Vertical line: border between low-resolution observations (every $0.5t_{\text{res}}$) for $t < 25t_{\text{res}}$ and higher-resolution observations (every $0.1t_{\text{res}}$) for $t > 25t_{\text{res}}$. Possible features in the latter range are likely due to the increased temporal resolution.

The coefficients relevant for the generation of \overline{B}_y^X (from $\overline{\mathcal{E}}_z^X$ only) are α_{31}^{11} , α_{32}^{11} , β_{313}^{11} and β_{323}^{11} . We have used the test-field method (see Sec. 3.2) to find them and present the results in Fig. 12. They turn out to be surprisingly large, when compared to the rms velocity (e.g., $(\alpha_{31}^c + \alpha_{31}^s)^{1/2} \gtrsim 4u_{\text{rms}}$) and some may show a trend across the transition from the α - Ω to the α^2 mode. This overall trend is hypothesized to be due to the increase in u_{rms} that accompanies the transition from a stronger α - Ω field to a weaker α^2 field with less potential to inhibit the flow. It is interesting that with the exception of α_{33}^{11} , the large transport coefficients are all those which generate an $\overline{\mathcal{E}}$ out of the \hat{x} -directed field, i.e. out of a field that feels the effect of shear. We speculate that these coefficients, with, themselves, explicit x -dependence, feel the shear quite strongly.

6. Discussion and conclusions

We have demonstrated that, while α^2 - Ω modes are kinematically preferred to α^2 modes in homogeneous systems that support both, the α^2 mode acts in a fratricidal manner against the former after the nonlinear stage has been reached. This transition can occur in at least two different fashions. Further, we have not observed the reverse process. One of the two transition processes, based on superposed α^2 - Ω and α^2 modes, operates in a basically deterministic fashion through a large-scale velocity pattern generated by the interaction of the modes. In contrast, we interpret the mechanism of the second process, which may start only many resistive times past the saturation of the α^2 - Ω dynamo, by assuming that both the α^2 - Ω and the α^2 modes are stable solutions of the nonlinear system. Transitions occur if due to the random forcing a sufficiently strong perturbation builds up which tosses the system out of the basin of entrainment of the α^2 - Ω mode into that of the α^2 mode. This hypothesis is bolstered by both the random timing of these transitions and by the large time-variability seen in the amplitude of the α^2 - Ω field. A

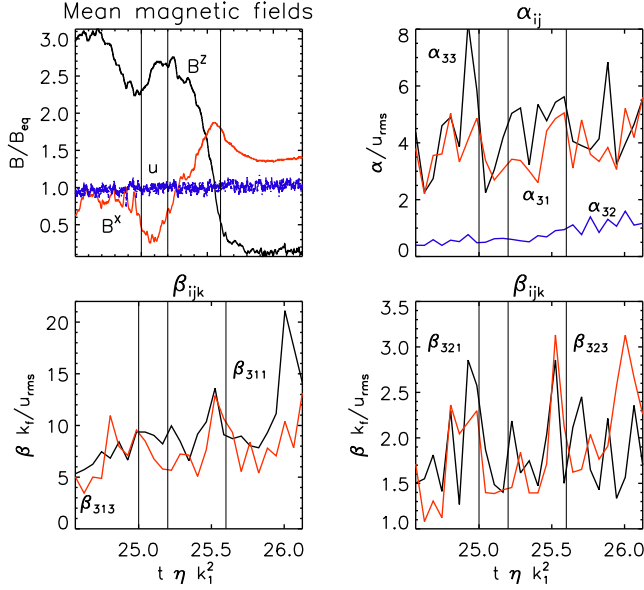


Fig. 12. Run H. Upper left panel: rms values of $\overline{B^x}$, $\overline{B^y}$ and u ($u_{\text{rms}} = \langle u^2 \rangle^{1/2}$), cf. Fig. 8. Remaining panels: Selected quadrupolar moments of α_{ij} and β_{ijk} determined by the test-field method and given by $(\alpha_{ij}^{c2} + \alpha_{ij}^{s2})^{1/2}$ (see Eq. (34)), likewise for β_{ijk} . Normalization is by the temporally averaged u_{rms} , as u_{rms} undergoes a slow, steady drift over time. Vertical lines mark the times of events visible in the first panel.

return seems to be much less likely as the level of fluctuations of the α^2 mode is, by contrast, greatly reduced.

These results fit with earlier work studying dynamos whose non-linear nature is fundamentally different from their linear one (e.g., Fuchs et al., 1999). While our simulations are limited to Cartesian, cubic, shearing-periodic domains, they are particularly exciting given that the only dynamo which has been observed over a long baseline and which could be either $\alpha-\Omega$ or α^2 , the solar dynamo, indeed shows differing modes of operation (regular cycles vs. deep minima). The results are also disturbing in that we have evidence for non-deterministic, rare (as they occur in scales of multiple resistive times or hundreds of turbulent turnovers) mode changes that show no evidence for a return. Given that the α^2 mode in our simulations seems much calmer than the $\alpha^2-\Omega$ mode, a rare random excursion in the field geometry is likely to be the initiating agent of the transition. While a bifurcation between different stable modes has long been an acknowledged possibility for dynamos (Brandenburg et al., 1989; Jennings, 1991), a rare, stochastic, possibly uni-directional transition is perhaps the most troublesome form of such bifurcations except for the ultimate self-extinction.

The $\alpha-\Omega$ dynamo is believed to be common and important for systems like the Sun or accretion disks, which all have long life-times compared to turbulent turnover times. It is then a daunting possibility that we could be forced to stretch our simulations over very long temporal base-lines to find the actual long-lasting field configuration. More positively, our result, while in a different geometry, increases the importance of recent work on non-oscillatory $\alpha-\Omega$ and oscillatory α^2 modes in spherical shells for the solar dynamo (Mitra et al., 2010; Schinner et al., 2011).

Acknowledgements. We acknowledge the allocation of computing resources provided by the Swedish National Allocations Committee at the Center for Parallel Computers at the Royal Institute of Technology in Stockholm and the National Supercomputer Centers in Linköping. This work was supported in part by the European Research Council under the AstroDyn Research Project No. 227952 and the Swedish Research Council Grant No. 621-2007-4064.

References

- Baryshnikova, I., & Shukurov, A. 1987, *Astron. Nachr.*, 308, 89
- Brandenburg, A. 2001, *ApJ*, 550, 824
- Brandenburg, A., & Subramanian, K. 2005, *Phys. Rep.*, 417, 1
- Brandenburg, A., Krause, F., Meinel, R., Moss, D., & Tuominen, I. 1989, *A&A*, 213, 411
- Brandenburg, A., Rädler, K.-H., & Schinner, M. 2008a, *A&A*, 482, 739
- Brandenburg, A., Rädler, K.-H., Rheinhardt, M., & Käpylä, P. J. 2008b, *ApJ*, 676, 740
- Charbonneau, P. 2010, *Living Rev. Solar Phys.*, 7, 3
- Christensen, U., Olson, P., & Glatzmaier, G. A. 1999, *Geophys. J. Int.*, 138, 393
- Eddy, J. A. 1976, *Science*, 286, 1198
- Fuchs, H., Rädler, K.-H., & Rheinhardt, M. 1999, *Astron. Nachr.*, 320, 129
- Grote, E., & Busse, F. 2000, *Phys. Rev. E*, 62, 4457
- Hubbard, A., & Brandenburg, A. 2009, *ApJ*, 706, 712
- Hubbard, A., Del Sordo, F., Käpylä, P. J., & Brandenburg, A. 2009, *MNRAS*, 398, 1891
- Jennings, R. L. 1991, *Geophys. Astrophys. Fluid Dyn.*, 57, 147
- Käpylä, P. J., & Brandenburg, A. 2009, *ApJ*, 699, 1059
- Mitra, D., Tavakol, R., Käpylä, P. J., & Brandenburg, A. 2010, *ApJ*, 719, L1
- Rädler, K.-H., & Bräuer, H.-J. 1987, *Astron. Nachr.*, 308, 101
- Rädler, K.-H., Wiedemann, E., Brandenburg, A., Meinel, R., & Tuominen, I. 1990, *A&A*, 239, 413
- Rheinhardt, M., & Brandenburg, A. 2010, *A&A*, 520, A28
- Schinner, M., Rädler, K.-H., Schmitt, D., Rheinhardt, M., Christensen, U. 2005, *Astron. Nachr.*, 326, 245
- Schinner, M., Rädler, K.-H., Schmitt, D., Rheinhardt, M., Christensen, U. R. 2007, *Geophys. Astrophys. Fluid Dyn.*, 101, 81
- Schinner, M., Pettdemange, L., & Dormy, E. 2010, *arXiv:1101.1837*
- Steenbeck, M., & Krause, F. 1969, *Astron. Nachr.*, 291, 49
- Stefani, F., & Gerbeth, G. 2003, *Phys. Rev. E*, 67, 027302